Case Studies in Thermal Engineering 8 (2016) 41–50

Contents lists available at ScienceDirect

Case Studies in Thermal Engineering

journal homepage: www.elsevier.com/locate/csite

Numerical and experimental study of a corrugated thermal collector

A. Álvarez [a,*], J. Tarrío-Saavedra [b], S. Zaragoza [c], J. López-Beceiro [c], R. Artiaga [c], S. Naya [b], B. Álvarez [d]

[a] Universidad de La Coruña, Departamento de Ingeniería Naval y Oceánica, Grupo PROTERM, Avd. Mendizábal s/n, 15403 Ferrol, La Coruña, Spain
[b] Universidad de La Coruña, Departamento de Matemáticas, Grupo MODES, Avd. Mendizábal s/n, 15403 Ferrol, La Coruña, Spain
[c] Universidad de La Coruña, Departamento de Ingeniería Industrial, Grupo PROTERM, Avd. Mendizábal s/n, 15403 Ferrol, La Coruña, Spain
[d] Universidad de La Coruña, Departamento de Economía Financiera y Contabilidad, Grupo PROTERM, Avd. Mendizábal s/n, 15403 Ferrol, La Coruña, Spain

ARTICLE INFO

Article history:
Received 2 October 2015
Received in revised form
16 March 2016
Accepted 22 March 2016
Available online 29 April 2016

Keywords:
Solar collector
Buildings
Parallel configuration
Numerical simulation
Nonparametric regression

ABSTRACT

The present work proposes a design for solar thermal collectors and also a numerical simulation analysis procedure to evaluate the collector performance. The performance of this collector is compared with the performance of other two commercial ones by observing both the numerical modeling study and experimental test results. Benefits of using the corrugated parallel approach, in terms of yield, are shown applying a new alternative approach of numerical modeling. A better performance is observed for the corrugated parallel collector, which provides a higher yield using an energy-absorbing surface. Moreover, the proposed numerical methodology could be used to evaluate the performance of other thermal collector configurations.

1. Introduction

The energy that a society consumes and its use and transformation effectiveness are criteria that characterize the development degree of a country. In fact correlations between the energy consume and the life quality levels have been defined and reported [1]. The development of the welfare society progress in parallel with the increasing energy consumption; for instance, the eighteenth century energy consumption per person was estimated about 3 kW h per day in buildings while nowadays is approximately 350 kW h per day in buildings, according to González [2]. This increasing consumption is causing sustainability, environmental, social and political problems. The described situation obviously requires corrective actions. Accordingly, the European Union has set a target for 2020 to reach the objective 20–20–20 (20% emissions reduction, 20% of energy provided by renewable energies, and 20% for saving energy). Focusing in an illustrative case, Spain is a paradigmatic example. In fact, this country is completely dependent on energy supply from abroad, importing the 75.6% of total consumption [3]. For correcting this, a contribution of renewable energy to gross final consumption of about 22.7% is expected to reach in 2020 [4]. Therefore, for achieving these objectives the design of increasingly efficient renewable devices in buildings as solar collectors is

* Corresponding author.
E-mail addresses: aalvarez@udc.es (A. Álvarez), jtarrio@udc.es (J. Tarrío-Saavedra), szaragoza@udc.es (S. Zaragoza), jorge.lopez.beceiro@udc.es (J. López-Beceiro), rartiaga@udc.es (R. Artiaga), salvador.naya@udc.es (S. Naya), balvarez@udc.es (B. Álvarez).

http://dx.doi.org/10.1016/j.csite.2016.03.007

Nomenclature

$(\tau\alpha)$	transmittance-absorptance product
$\dot{m}$	collector flow rate (kg/s)
η	efficiency
η_i	instantaneous efficiency
$\boldsymbol{n}$	unit normal vector to the boundary (positive outward)
ρ	density, (kg/m^3)
a_1	linear heat loss coefficient, (W/(m^2 K))
a_2	quadratic heat loss coefficient, (W/(m^2 K^2))
A_c	collector area, (m^2)
C_p	specific heat, (J/(kg K))
D_h	hydraulic diameter, (m)
NU_D	diameter Nusselt number
e_c	collector thickness, (m)
e_{in}	insulation thickness, (m)
ε	emittance
h_f	fluid-to-tube heat transfer coefficient, (W/(m^2 K))
k	thermal conductivity, (W/(m K)) and number of ducts
k_{in}	insulation thermal conductivity, (W/(m K))
L	length duct section, (m)
N	number of glass covers
P_c	perimeter collector, (m^2)
q_I	incident solar irradiance on tilted surface, (W/m^2)
q_S	absorbed irradiance, (W/m^2)
T	temperature, (°C)
t	time, (s)
T_a	ambient temperature, (°C)
T_{fi}	inlet fluid temperature, (°C)
T_{fm}	mean fluid temperature, (°C)
U_i	back loss coefficient, (W/(m^2 K))
U_l	edge loss coefficient, (W/(m^2 K))
U_t	top loss coefficient, (W/(m^2 K))
w	fin width, (m)

needed. Accordingly, the aim of this work is the proposal of a new solar thermal corrugated collector with parallel configuration for buildings that improves other commercial panel efficiency.

The tube and plate absorbers have been studied by analytical methods by several authors [5–8]. The study of Hottel and Woertz is a pioneer work in the field [5]. Duffie and Beckman [6] presented the theory of flat-plate and concentrating collectors relating this topic with solar process economics and solar heating design. Eisenmann et al. [7] focuses on the correlations between the efficiency factor and the material content of absorber and tubing for flat-plate collectors with the fin-and-tube geometry, and Eismann and Prasser [8] calculated the efficiency of non-ideal absorbers using two-dimensional simulations and proposed new correlation for the fin efficiency to provide accurate efficiency/cost optimization. Moreover, numerical analysis is nowadays an essential tool to evaluate these types of devices [9–20]. Namely, in [9] block-oriented simulation technique was applied to obtain the solution of the dynamic model performed to describe the thermal behavior of solar collectors, while in [10] new transfer functions based on a validated collector model were performed to control collectors used in domestic applications. In these studies, mathematical models are developed to simulate numerically the collector performance using Matlab and FEM. The numerical simulation permits to know the collector yields without performing additional experimental tests. It is indispensable to predict the collector performance under a wide variety of conditions, in different operating scenarios. In addition, in the most of these works the simulations have been validated by experimental measurements.

Otherwise, the application of statistical learning tools is needed to properly estimate the collector characteristics from experimental data. Inference techniques applied to regression model are absolutely necessary to estimate dependence relationships and then make predictions [21,22]. Namely, multiple linear regression models (black-box type model) are proposed to describe the transient collector processes precisely [23]. However, the application of nonparametric models is not as common in this field. They are more flexible and simple ways to estimate regression functions. In the present work, a smoothing method that uses a spline function to fit a set of noisy observations is used [21,24]. Moreover, the uncertainty of experimental observations can be nowadays obtained by bootstrap techniques [25–27] and thus can be applied to thermal collector measurements. Bootstrap is a simple and straightforward way to estimate confidence intervals, variance,

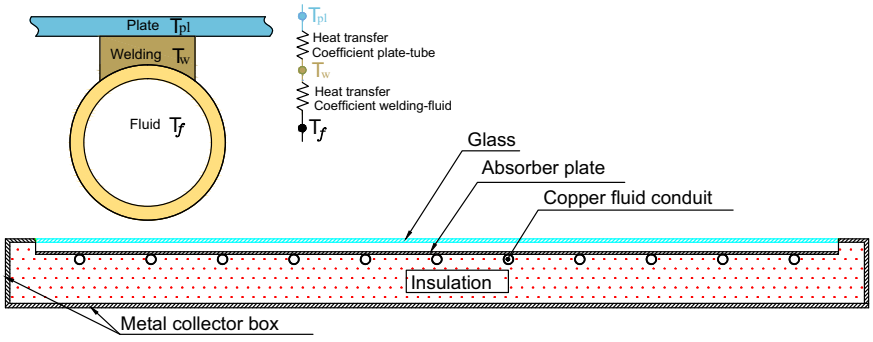

Fig. 1. Scheme of a standard flat-plate solar collector.

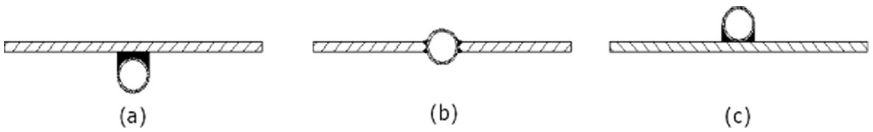

Fig. 2. Positions of the tube containing the fluid respecting to the absorbent plate: (a) welded underneath the plate, (b) welded between plate, and (c) welded above the plate.

correlation coefficients, odds ratio, misclassification errors, etc. just from data sample and resampling [25–27]. This study provides the performance results corresponding to a new corrugated collector design with parallel configuration, thinking of using new alternatives for numerical simulation. An additional comparison using simulated and experimental data shows the new collector design is more efficient than two commercial flat- plate collectors. Since the thermal plates are intended to be installed in buildings placed in northern Spain, obtaining higher collector efficiency factor is crucial due to the relatively lower solar irradiation level in this area.

2. Comparison between standard and corrugated solar thermal collector

A standard thermal solar collector is generally composed of a metal housing which should ensure water tightness. In the upper frame, hardened glass with low iron content is situated which facilitates the transmission of radiation up to 95% and presents a thickness of about 4 mm. Inside the black absorbing plate is placed. Note that there are copper tubes with a thickness of about 5–6 mm welded to the plate, through which the heat transfer fluid is transported as Fig. 1 shows. Under the plate an insulating material, commonly mineral wool is placed. These channels through which the heat transfer fluid circulates can present parallel flow or serpentine typology. Fig. 1 plots a diagram of a standard low temperature level corresponding to a solar thermal collector, while Fig. 2 shows its different positions relative to the duct plate.

It is important to stress that the material used for making the tubes and the absorber plate of the proposed new design differs from the materials used in the commercial thermal solar collectors. Namely, aluminum is used in the new design instead cooper, currently utilized in standard solar panels, due its lower prize. It is necessary to emphasize the novelty of the ducts design (see Fig. 3) which allows the fluid to present a larger contact surface regarding to the absorber plate, even higher than in other sandwich type collectors.

3. Experimental setup

In order to compare, experimental results were obtained from two commercial collectors (see Fig. 4). In this experimental steep two thermal solar panels were connected. The first one is a Brown Boveri Corporation product, hereafter referred as BBC, defined by a sun surface exposure equal to 1.14 m^2. The second one is a Roth Werke product, hereafter named as Roth, characterized by a sun surface exposure of 2.27 m^2.

The heat transport medium is composed of a 30 vol% solution of ethylene glycol in water. This medium is impulsed by a N.2 07 13 (DAB SPA pump). It is a 78 W pump, which allows controlling the flow in the range from 16 to 29 l min^{-1}. A 16 l min^{-1} flow rate was used for all experiments. The physical properties of aluminum, the insulation material, and the heat fluid can be consulted in Table 3. The experimental equipment was pointing southwards fixing an angle of 35° regarding to the soil (see Fig. 4). This device was placed at the following geographic coordinates: latitude 43.236373° and longitude −7.559752°. The measurements were obtained between 12:00 (GMT +01:00) and 16:00 (GMT +01:00) in September. In addition, the temperature was controlled with an accuracy of 0.1 °C by means of Crison thermometers.

4. Numerical simulation for corrugated parallel configuration

A two-dimensional modeling is made to evaluate the effect of different parameters on the behavior of the system. To obtain the temperature distribution corresponding to two-dimensional model geometric shown in Fig. 5, the heat equation

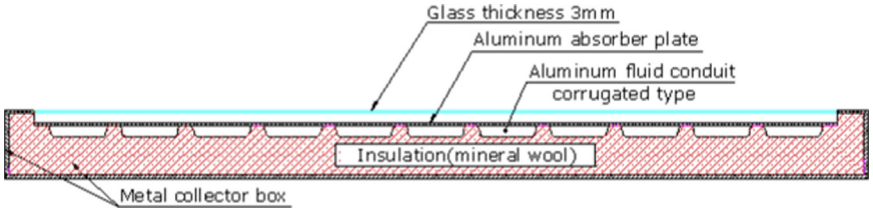

Fig. 3. Scheme of a new thermal solar collector.

Fig. 4. Collectors facing south, inclination 35°.

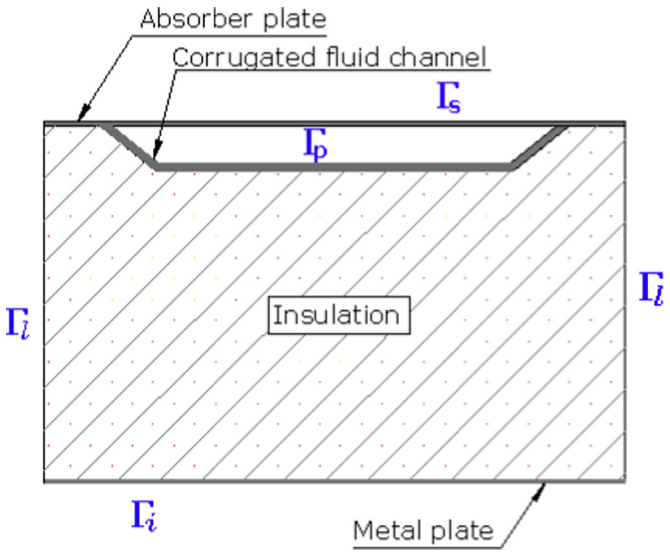

Fig. 5. Computational domain W.

is solved and expressed as:

$$-\nabla\cdot(k\nabla T) = 0 \ \text{ in } \Omega \tag{1}$$

where T is the temperature and k is the thermal conductivity.

This partial differential equation has to be supplemented by the following boundary conditions:

1. Convective boundary condition at the inner perimeter of the tube through which fluid flows

$$k\frac{\partial T}{\partial \boldsymbol{n}} = h_f(T_{fm} - T) \ \text{ over } \ \Gamma_p, \tag{2}$$

where h_f is the heat transfer coefficient corresponding to the tube-fluid, T_{fm} the mean fluid temperature at the halfway, and Γ_p the contour of the tube through which fluid flows (see Fig. 5).

2. The boundary condition at the absorbing plate of the collector, taking into account the absorbed solar irradiance, q_s, and the thermal losses from the collector to the environment is

$$k\frac{\partial T}{\partial \boldsymbol{n}} = q_s + U_t(T_a - T) \ \text{ over } \ \Gamma_s, \tag{3}$$

where T_a represents the ambient temperature, and Γ_s is that part of the absorber plate contour that receives solar radiation (see Fig. 5).

3. And finally, the convective boundary conditions, including loss to the sides and the bottom

$$k\frac{\partial T}{\partial \boldsymbol{n}} = U_i(T_a - T) \ \text{ over } \ \Gamma_i \tag{4}$$

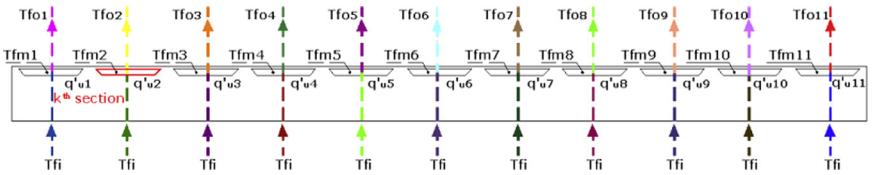

Fig. 6. Cross-section of the collector. (For interpretation of the references to color in this figure, the reader is referred to the web version of this article.)

$$k\frac{\partial T}{\partial \boldsymbol{n}} = U_l(T_a - T) \text{ over } \Gamma_l, \tag{5}$$

where U_i and U_l are the heat loss coefficients of convective back and edge, respectively. These coefficients are calculated on the basis of the insulation thickness and the thermal conductivity. In this regard, the thickness of insulation at the bottom and the sides is considered the same. To obtain these coefficients, the Duffie and Beckman expressions are used [6]. They are given by

$$U_i = \frac{k_{in}}{e_{in}}, \tag{6}$$

$$U_l = \frac{(k_{in}/e_{in})P_c e_c}{A_c}, \tag{7}$$

where k_{in} is the thermal conductivity insulation, e_{in} the thickness insulation,P_c the perimeter of the collector, e_c the collector thickness and A_c the collector area.

For a parallel configuration (see Fig. 6) the inlet temperature of each conduit is the same. Thus, the boundary condition (2) is completed calculating the fluid average temperature in each corrugation using the expression

$$T_{fmk} = \frac{q'_{uk}L_k}{2\dot{m}Cpf} + Tfi, \tag{8}$$

where L_k is the length of each duct section, q'_{uk} is the useful heat transferred to the fluid per length in each section of the duct wall, and k accounts for the number of ducts.

The transient numerical simulation is solved using the mesh of computational domain depicted in Fig. 6. It is composed of twenty two nodes, eleven defined by the intervals $[i_k, c_k]$, and the remaining eleven accounted for the intervals $[c_k, o_k]$. The i_k and o_k symbols depict the in and out points, respectively, corresponding to the k^{th} cross section, with $k=1\ldots.11$. These ducts are properly represented in the scheme shown in Fig. 6. Each stretch is labelled by one specific color, in order to correctly identify each one of the overall twenty two meshes.

Next, Tables 1 and 2 indicate the geometric values and experimental operations for calculating the boundary conditions. In addition, Table 3 shows the physical properties values corresponding to the AW 1050 series aluminum used in making the prototype, the heat fluid (water-30% ethylene glycol) and the insulation material (mineral wool).

5. Results and discussion

Since the numerical problem is solved, the instant efficiency under stationary conditions can be calculated from an input fluid temperature range T_{fi} between 15 °C and 100 °C, at fixed ambient temperature, T_a 20 °C. The Fig. 7 shows the characteristic curve for a corrugated, BBC and Roth collectors with parallel configuration. The efficiency corresponding to the corrugated collector is slightly higher than the efficiencies of commercial collectors (Fig. 7). The curve for corrugated collector can be obtained using the expression (9) [28] fitted to efficiency data. The model parameters are obtained using the least-squares method.

$$\eta = 0.8602 - 2.4898\frac{T_{fi}-T_a}{q_l} - 0.0070052\frac{(T_{fi}-T_a)^2}{q_l}. \tag{9}$$

This polynomial fit model provides the heat loss coefficients $a_1=2.4898$ W/m^2 K and $a_2=0.007052$ W/m^2 K^2, according to EN 12,975-2:2006 [28]. Table 4 shows the values obtained for the significant parameters for this specific collector. The maximal yield obtained by the model corresponding to

Table 1
Geometrical data corresponding to the corrugated collector.

Geometrical parameters	Value
Collector area, A_C	1 m^2
Collector thickness, e_c	0.08 m
Collector perimeter, P_c	4 m
Insulation thickness, e_{in}	0.03 m

Table 2
Operational conditions of the corrugated collector.

Physical parameters	Value
Transmittance-absorptance, $\tau\alpha$	0.874
Incident solar irradiance, q_I	1000 W/m^2
Ambient temperature, T_a	20 °C
Inlet fluid temperature, T_{fi}	15 °C
Flow rate, $\dot{m}$	0.01 kg/s

Table 3
Physical properties of the aluminum alloy, heat fluid and insulation material from which the new corrugated collector is composed.

	Aluminum	Fluid	Insulation
Density, kg/m^3	2700	999.5	100
Specific heat, J/kg K	900	4190	1000
Thermal conductivity, W/m K	160	–	0.07

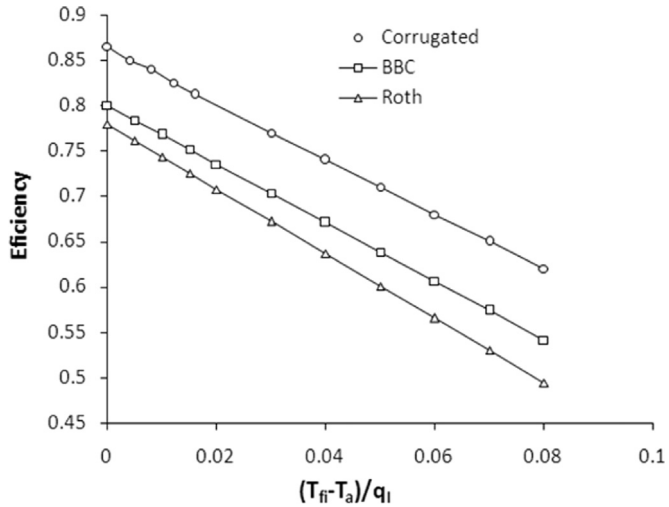

Fig. 7. Instantaneous efficiency for corrugated, BBC and Roth collectors with parallel configuration.

Table 4
Characteristics values corrugated collector with parallel configuration.

Description	at T_a=20 °C
Efficiency	86%
Mean superficial temperature	23.1 °C
Overall loss coefficient	3 W/m^2 K
Collector heat removal factor	0.98

expression (9) is equal to 86%, while the BBC and Roth collector yields are 80% and 77.9%, respectively. The efficiency values corresponding to the BBC and Roth collectors have been obtained from their commercial catalogues. Both commercial collector present high yields, but the highest corresponds to the proposed design.

Moreover, Fig. 8 shows the yield linked to three different incident radiation levels on the collector. They correspond to an average day in summer, autumn-spring, and winter, respectively. Therefore, the yield values of the corrugated collector with parallel configuration can be easily obtained for any temperature using the information in Fig. 8. The gap between the summer and winter yields is not higher than 6%.

A nonparametric regression model based on tin plate splines is applied to estimate the Roth and BBC efficiency curves obtained from experimental data [29]. The efficiency uncertainties corresponding to the Roth and BBC collectors are estimated using bootstrap confidence intervals [26,29] at a 95% confidence level (see Fig. 9). These statistical tools can be easily applied using the mgcv [29] library, belonging to R free statistical software [30]. Fig. 9 shows these results and offers a comparison with the efficiency curve obtained by numerical simulation corresponding to the proposal collector. The efficiency values obtained from the numerical study of the corrugated parallel collector are always higher than the obtained values for BBC and Roth collectors. These numerical simulation values are out of the confidence intervals built for the BBC and Roth collectors, thus we can consider that corrugated collector results are statistically different from the others. It is important to note that if the corrugated and BBC collectors are compared, the efficiency difference is quite slighter.

The efficiency curve of the corrugated collector with parallel configuration presents the same behavior as the BBC and Roth collectors, although the surface exposed to solar radiation of the corrugated collector is 12% lower than that of the BBC collector and 56% lower than the Roth collector, as pointed in

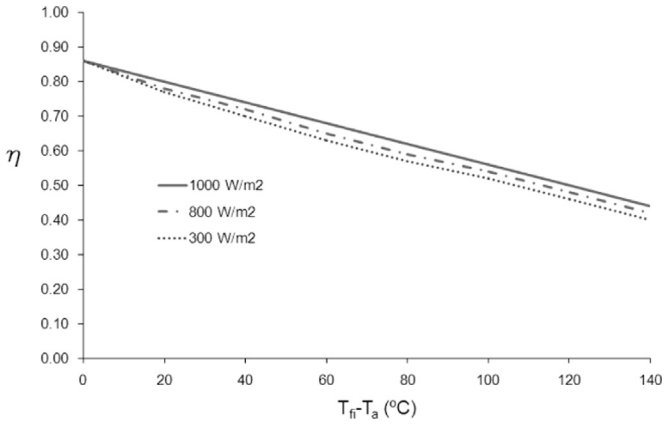

Fig. 8. Corrugated collector yield for three characteristic irradiances.

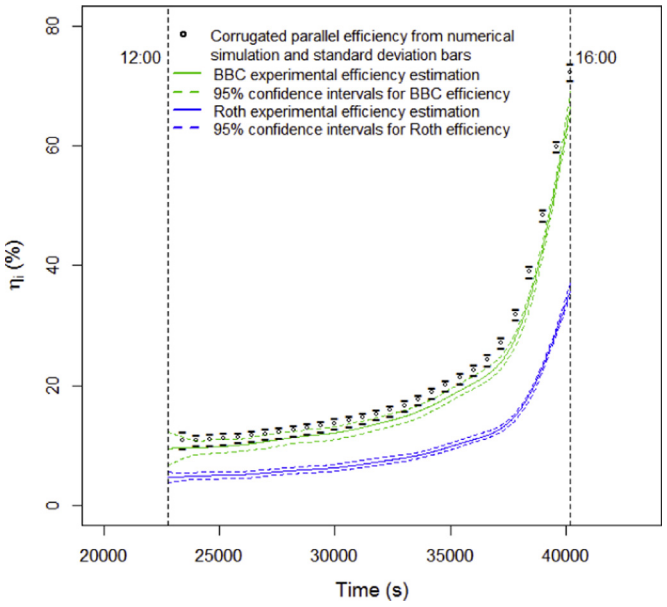

Fig. 9. Comparison of instantaneous efficiency with experimental data and bootstrap confidence bands between the BBC and Roth collectors, and the corrugated collector (numerical simulation data). Numerical and experimental measurements begin at 12:00 (GMT +01:00).

the second section. The model was run under the same conditions that the experimental test in order to obtain the parameters that characterized the design and optimization such as thermal efficiency.

Evolutionary data corresponding to solar irradiance and ambient temperature are used in order to solve numerically the transient thermal problem and compare the numerical simulation results of the new design with those corresponding two commercial collectors (see Fig. 10). Ambient data were obtained by a meteorological station next to the place where experimental testing for standard collectors where performed.

Furthermore, the values provided by MeteoGalicia agency [31] correspond to the horizontal global solar radiation. Thus, the necessary conversions using the equations proposed by Duffie and Beckman [6] must be implemented to obtain the data corresponding to radiation on a 35° inclined surface, oriented southward (the slope of the Roth and BBC panels in the experimental setup).

Fig. 11 represents a three-dimensional transient numerical simulation for a corrugated collector with parallel configuration (this figure is obtained directly of the software Comsol Multiphysics). The developed model shows that the temperature increasing in each tube is practically the same.

6. Conclusions

A corrugated solar design with parallel configuration has been successfully proposed. Its performance has been compared with other current solar collectors such as Roth and BBC. The three typologies provide high efficiency values but the proposed design presents the highest one. Thus, the yield obtained by the proposed model is equal to 86%, while the yield corresponding to the BBC and Roth collectors are 80% and 77.9%, respectively. This result is more significant assuming that the new model just represents 88% the surface of BBC collector and 44% the surface in the case of collector Roth. This

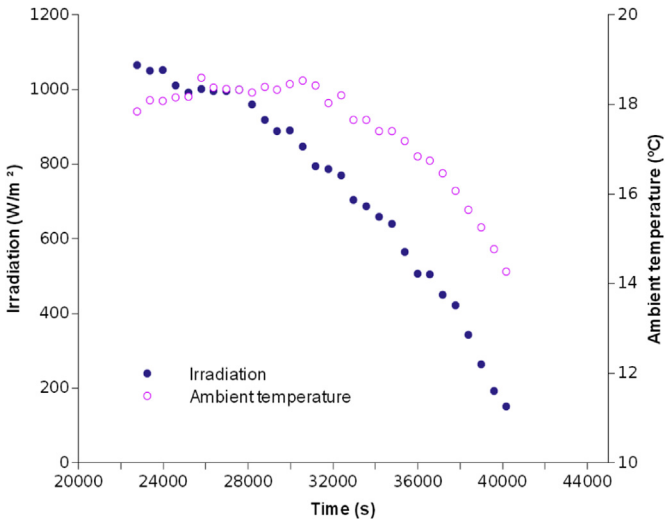

Fig. 10. Ambient temperature and irradiation obtained at the day where the experimental data were obtained.

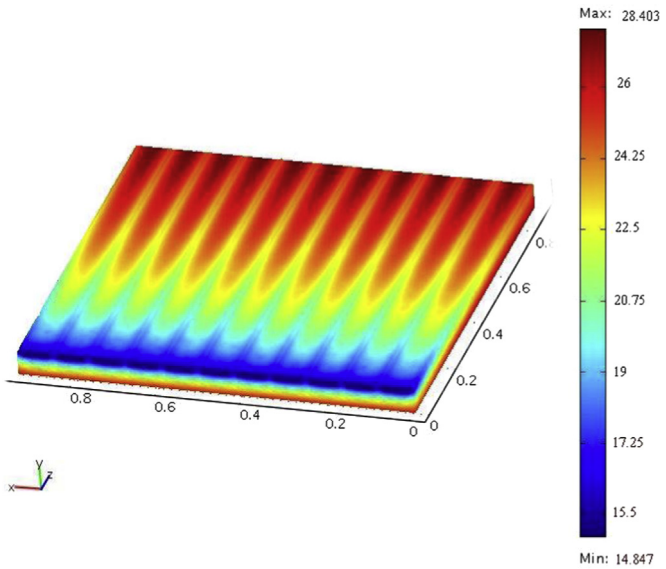

Fig. 11. Three-dimensional distribution of temperature in corrugated transient thermal collector with parallel configuration.

advantage is obtained due to its novel design of corrugated conduits, which increases the contact surface between the carrier fluid and the absorber plate. It is also important to note that the experimental instantaneous efficiency for Roth and BBC collectors and the results obtained from the numerical simulation for corrugated collector are very similar, especially those from the BBC and corrugated collector. Therefore, the numerical simulation provides reliable results, close to reality. But the proposed corrugated design presents the highest instantaneous efficiency during all the test day. This result supports the development of the proposed corrugated collector and its application in any place where hot water is required such as buildings and cruise ships. In addition, the proposed numerical methodology has provided properly the main parameters that characterize the thermal behavior of the corrugated collector with parallel configuration. This simulation procedure can be applied to other collector geometries for buildings.

Acknowledgments

This research has been partially supported by the Spanish Ministry of Science and Innovation. Grants MTM2011-22392 (ERDF included), MTM2014-52876-R and ENE2013-48015-C3-1-R.

Appendix

This appendix is composed of some definitions which can be found in [17] to clarify some points of the present study. To compute the top loss coefficient U_t we have used the empirical equation proposed in Duffie and Beckman [6] which expresses a nonlinear and non local dependence with respect to the mean temperature of the absorbing plate

$$Ut = \left\{ \frac{N}{\frac{C}{T_{pm}}\left[\frac{(T_{pm}-T_a)}{(N+f)}\right]^e} + \frac{1}{h_w} \right\}^{-1} + \frac{\sigma(T_{pm}+T_a)(T_{pm}{}^2+T_a^2)}{(\varepsilon_c + 0.00591N{\cdot}h_w)^{-1} + \frac{2N+f-1+0.133\varepsilon_c}{\varepsilon_g} - N}$$

where N is the number of glass covers, ε_g emittance of glass (0.88), ε_c emittance of plate, $T_a$ambient temperature, T_{pm} mean plate temperature given by $T_{pm} = \int_{\Gamma_S} Td\sigma/w$ denoted by Γ_S top absorber plate and w the fin width.

h_w wind heat transfer coefficient,.

β collector tilt,

$$f = (1 + 0.089h_w - 0.1166h_w{\cdot}\varepsilon_c)(1 + 0.07866N),$$

$$C = 520(1 - 0.000051\beta^2), \quad (0^o < \beta < 70^o),$$

$$e = 0.430(1 - 100T_{pm}^{-1}),$$

σ Stefan-Boltzmann constant.

When calculating losses outwards we must also take into account the plate losses plate due to the wind exposition and these are obtained with the equation

$$h_w = 2.8 + 3v$$

where v is the wind velocity.

On the other hand, denoting by q'_u the useful heat transferred to the fluid along the tube per unit length in the flow direction

$$q'_u = \int_{\Gamma_P} k\frac{\partial T}{\partial \boldsymbol{n}} d\sigma$$

the energy equation can be written as

$$\dot{m}\ cp\frac{dTf}{dz} = q'_u$$

being $Tf\ (z)$ the temperature of the fluid at the point z. However, considering Tfi as the fluid inlet temperature and integrating the ordinary differential equation one gets

$$Tf(z) = \frac{\int_0^z q'_{u(\zeta)} d\zeta}{\dot{m}cpf} + Tfi$$

Further, assuming that q'_u is constant in [0, L] the mean fluid temperature can by calculated as

$$Tfm = \frac{q'_u L}{2\dot{m}cpf} + Tfi$$

where L is the duct length.

Substituting in Eq. (2) the average temperature of the fluid by the expression Tfm, the following expression is just obtained

$$k\frac{\partial T}{\partial \boldsymbol{n}} = h_f\left(\frac{q'_u L}{2\dot{m}C_{pf}} + T_{fi} - T\right),$$

and integrating this expression on the duct boundary we get

$$q'_u(1-a) = \int_{\Gamma_P} h_f(T_{fi} - T)d\sigma$$

where $a = \int_{\Gamma_P} h_f L/(2\dot{m}C_{pf})d\sigma$.

In the case of $a \neq 1$ the Eq. (2) becomes a non-local boundary condition formulated as

$$k\frac{\partial T}{\partial \boldsymbol{n}} = \frac{h_f L}{2\dot{m}cpf}\frac{\int_\Gamma h_f(T_{fi}-T)d\sigma}{(1-a)} + h_f(T_{fi}-T).$$

expressed in terms of the duct boundary and on the inlet fluid temperature. To conclude with the boundary conditions, they

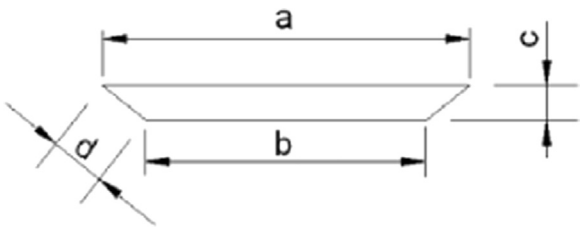

Fig. 12. Duct geometry.

are assumed adiabatic at bottom and edges.

With the purpose of defining the boundary conditions (2) and (3), the heat transfer coefficient is calculated between fluid and corrugated in terms of the diameter and Nusselt number as (see [6])

$$h_f = \frac{k_f Nu_D}{D_h}$$

where D_h is the hydraulic diameter which is defined as $D_h = 4(A_S/p_m)$; being $A_s = c((a+b)/2)$ section area and $p_m = a + b + 2d$ wetted perimeter of the duct section (see Fig. 12). The Nusselt number Nu_D is given by the semi-empirical relationship provided by Hausen [32] assuming fully developed laminar flow. This relationship takes into account the length of conduit.

References

[1] S. Kalogirou, Solar Energy Engineering processes and Systems, Elsevier, London, 2009.
[2] J. González, Energías Renovables, Reverté, Barcelona, 2009.
[3] Ministerio de Industria, Energía y Turismo, La energía en España 2011, Ministerio de Industria, Energía y Turismo, Centro de publicaciones, Madrid, 2012.
[4] Instituto para la Diversificación y Ahorro de la Energía, Plan de Energías Renovables 2011 – 2020, Available online: ⟨http://www.idae.es/index.php/id.670/relmenu.303/mod.pags/mem.detalle⟩, 2014 (accessed 06/10/2014).
[5] H.C. Hottel, B.B. Woertz, Performance of flat-plate solar heat collectors, Trans. ASME (1942) 64–91.
[6] J.A. Duffie, W.A. Beckman, Solar Engineering of Thermal Process, Wiley Inter-Science, New York, NY, 1991.
[7] W. Eisenmann, K. Vajen, H. Ackermann, On the correlations between collector efficiency factor and material content of parallel flow flat-plate solar collectors, Sol. Energy 76 (2004) 381–387.
[8] R. Eismann, H.M. Prasser, Correction for the absorber edge effect in analytical models of flat plate solar collectors, Sol. Energy 5 (2013) 181–190.
[9] Y.L. Shuli, Numerical study on thermal behaviors of a solar chimney incorporated with PCM, Energy Build. 80 (2014) 406–414.
[10] J. Buzás, R. Kicsiny, Transfer functions of solar collectors for dynamical analysis and control design, Renew. Energy 68 (2014) 146–155.
[11] K. Touafeka, M. Haddadib, A. Malekc, Design and modeling of a photovoltaic thermal collector for domestic air heating and electricity production, Energy Build. 59 (2013) 21–28.
[12] M. Hassan, Y. Beliveau, Design, construction and performance prediction of integrated solar roof collectors using finite element analysis, Constr. Build. Mater. 21 (2007) 1069–1078.
[13] D. Henderson, H. Junaidi, T. Muneer, T. Grasssee, J. Currie, Experimental and CFD investigation of an ICSSWH at various inclinations, Renew. Sustain. Energy Rev. 11 (2007) 1087–1116.
[14] M. Hassan, Y. Beliveau, Modeling of an integrated solar system, Build. Environ. 43 (2008) 804–810.
[15] N. Molero, J.M. Cejudo, F. Domínguez, E. Rodríguez, A. Carrillo, Numerical 3-D heat flux simulations on flat plate solar collectors, Sol. Energy 83 (2009) 1086–1092.
[16] J. Cadafalch, A detailed numerical model for flat-plate solar thermal devices, Sol. Energy 83 (2009) 2157–2164.
[17] A. Álvarez, O. Cabeza, M.C. Muñiz, L.M. Varela, Experimental and numerical investigation of a flat-plate solar collector, Energy 35 (2010) 3707–3716.
[18] M.A. Ahmed, M.Z. Yusoff, K.C. Ng, N.H. Shuaib, Numerical and experimental investigations on the heat transfer enhancement in corrugated channels using SiO_2–water nanofluid, Case Stud. Therm. Eng. 6 (2015) 77–92.
[19] Z. Ge, H. Wang, H. Wang, S. Zhang, X. Guan, Exergy analysis of flat plate solar collectors, Entropy 16 (2014) 2549–2567.
[20] C. You, W. Zhang, Z. Yin, Modelling of fluid flow and heat transfer in a though solar collector, Appl. Therm. Eng. 54 (2013) 247–254.
[21] P.J. Green, B.W. Silverman, Nonparametric Regression and Generalized Linear Models, CRC Press, 1994.
[22] T.J. Hastie, R.J. Tibshirani, Generalized Additive Models, Chapman Hall, 1990.
[23] R. Kicsiny, Multiple linear regression based model for solar collectors, Sol. Energy 110 (2014) 496–506.
[24] C. De Boor, A Practical Guide to Splines (Revised Edition), Springer, 2001.
[25] B. Efron, Better Bootstrap Confidence Intervals, J. Am. Stat. Assoc. 82 (1987) 171–185.
[26] B. Efron, R. Tibshirani, An Introduction to the Bootstrap, Chapman & Hall/CRC, Boca Ratón, 1993.
[27] H. Varian, Bootstrap Tutorial, Math. J. 9 (2005) 768–775.
[28] EN 12975-2:2006, Thermal solar systems and components – solar collectors – Part 2: test methods, Beuth Verlag, Berlin, 2006.
[29] S.N. Wood, Generalized Additive Models: An Introduction with R, Chapman And Hall, Boca Raton, 2006.
[30] R Development Core Team, R: A Language and Environment for Statistical Computing, R Foundation for Statistical Computing: Vienna, Austria, Available from: ⟨http://www.R-project.org⟩, 2014 (accessed 09/02/2015).
[31] MeteoGalicia, Spain: Xunta de Galicia, Conselleria de medio ambiente, territorio e infraestructuras, Available at: ⟨http://www.meteogalicia.es⟩, 2014 (accessed 09/02/2015).
[32] A.J. Chapman, Fundamentals of Heat Transfer, Macmillan Publishing Company, New York, 1987.